Available online at www.sciencedirect.com
ScienceDirect
Journal of Solid State Chemistry 179 (2006) 3989–3996
JOURNAL OF SOLID STATE CHEMISTRY
www.elsevier.com/locate/jssc

Mixed-metal flux synthesis of quaternary $RMn_2Tr_xZn_{20-x}$ compounds with Tr = Al, In

Evan M. Benbow, Susan E. Latturner*

Department of Chemistry and Biochemistry, Florida State University, Tallahassee FL 32306, US

Received 16 June 2006; received in revised form 1 September 2006; accepted 1 September 2006
Available online 16 September 2006

Abstract

Eighteen new intermetallic compounds $RMn_2Tr_xZn_{20-x}$ ($2<x<7$; R = rare-earth metal; Tr = Al, In) were synthesized using low-melting mixtures of (Tr/Zn) as a solvent. Structural refinement using single-crystal X-ray diffraction data shows that the compounds are substituted variants of the cubic $CeCr_2Al_{20}$-type structure (Fd-3m, $Z = 8$; unit cell parameters vary from $a = 14.1152(3)$Å for $YbMn_2Al_{5.3}Zn_{14.7}$ to $a = 14.8125(4)$Å for $SmMn_2In_{5.9}Zn_{14.1}$). The Zn and Tr elements show site preferences in the indium compounds, but not in the aluminum analogs. The substitution of trielide element for zinc modifies the valence electron count of the compounds to allow for the incorporation of Mn into the structure. Magnetic susceptibility data show no evidence of magnetic ordering down to 3 K.

Keywords: Eutectic; Flux; Intermetallic; Rare Earth; Zinc; Triel; Manganese; Indium; Aluminum

1. Introduction

Eutectic mixtures of elements form melts at temperatures lower than the standard melting point of the elements; synthesis in such media is of interest as it may produce materials with fewer defects and much less thermally produced strain than those synthesized using traditional high-temperature methods. These low-melting molten metal fluxes help facilitate diffusion of the elements in solution and make it possible for easy removal of excess materials used for synthesis by centrifugation. In addition, molten metal fluxes can often getter impurities, thus offering a cleaner environment for growth [1]. We have investigated In/Zn (96.2: 3.8 mol%, m.p. 143.5 °C) and Al/Zn (11.3%: 88.7%, m.p. 381 °C) eutectics for the growth of new intermetallic phases not accessible by traditional solid-state reactions. Optimization of the reactions required varying the ratios around the eutectic point; therefore, materials were synthesized in low-melting mixtures near the eutectic.

There are several families of ternary intermetallic phases comprised of a rare earth (R), a transition metal (T), and either Zn, In, or Al. These include $R_2T_3Zn_{14}$ (ordered Th_2Zn_{17} type), $R_6T_4Al_{43}$, $R_2Pt_7In_{16}$, and many others [2]. There appears to be no information available at the moment on quaternary compounds comprised of a rare-earth element (R), a transition metal (T), zinc, and an element of the boron group (trielide, Tr). In this work, reactions of rare-earth elements and Mn in both (In/Zn) and (Al/Zn) molten metal fluxes produced quaternary compounds with identical structure type and similar stoichiometries, $RMn_2Tr_xZn_{20-x}$ ($2<x<7$). The products can be described as substituted variants of the ternary $CeCr_2Al_{20}$ structure, although the indium-containing phases do show some site preferences indicative of a true quaternary structure.

There have been numerous $CeCr_2Al_{20}$-type ternary compounds synthesized (cubic space group Fd-3m, no. 227) with high amounts of aluminum (RT_2Al_{20}) and high amounts of zinc (RT_2Zn_{20}).[3,4] However, the aluminides are formed with the early transition metals T = Ti, V, Nb, Ta, Cr, Mo, and W, and the corresponding zinc compounds contain late transition metals T = Fe, Ru, Co, Rh, and Ni. Here we report the eutectic flux synthesis of

*Corresponding author. Fax: +1 850 644 8281.
E-mail addresses: ebenbow@chem.fsu.edu (E.M. Benbow), latturne@chem.fsu.edu (S.E. Latturner).

0022-4596/$ - see front matter © 2006 Elsevier Inc. All rights reserved.
doi:10.1016/j.jssc.2006.09.001

quaternary compounds that contain high amounts of zinc with aluminum (RMn$_2$Al$_x$Zn$_{20-x}$) and indium (RMn$_2$In$_x$Zn$_{20-x}$) incorporations, with middle transition metal Mn. We have also been able to incorporate Fe into this structure and will report on those results in a later publication.

2. Experimental procedure

2.1. Synthesis

Compounds with the formula RMn$_2$(In$_x$Zn$_{20-x}$) were synthesized by combining elements in a .5:1:(8:2) (m.p. 280 °C) millimolar ratio. Starting materials for the preparation of these compounds were chips and powders of the rare-earth elements (Metall, Strem, Cerac, Arris Int., all >99.9%), powders of Mn (Cerac, 99.9%), Zn (Fisher Chemical, 99.9%), Y (Cerac, 99.9%), and In shot (Alfa Aesar, 99.9%). All elements were combined in an alumina crucible which was placed in a fused silica tube; another alumina crucible was filled with silica wool and inverted on top of the reaction crucible in the silica tube to act as a filter during centrifugation. The fused silica tube was sealed under a vacuum of 10^{-2} Torr, and then heated to 900 °C for 10 h, held at this temperature for 24 h, then cooled to 800 °C in 20 h. The samples were then annealed for 24 h at 800 °C, cooled to 500 °C in 60 h, then held at this temperature for 12 h before cooling to 350 °C in 15 h. At 350 °C, the fused silica ampules were then inverted and placed into a centrifuge to remove excess molten flux.

Aluminum analogs of these compounds RMn$_2$(Al$_x$Zn$_{20-x}$) were synthesized with Al powder (Strem, 99.9%) instead of In shot. This was accomplished by combining elements in a .5:1:(2:10) (m.p. 400 °C) millimolar ratio. These reactions were prepared under the same conditions and starting materials as before except with a modified heating profile. The samples were heated to 1000 °C and held there for 24 h, then cooled to 800 °C in 40 h; again the temperature was held constant for 24 h and then cooled to 500 °C in 60 h. Samples were then centrifuged as before.

The crystals formed as cubes up to 3 mm on a side, typically in large conglomerations. Aluminide crystals have a shiny metallic luster whereas the indides have a dull luster. Elemental analysis was performed on all samples using a JEOL 5900 scanning electron microscope (SEM) with energy dispersive spectroscopy (EDS) capabilities. Samples were analyzed using a 30 kV accelerating voltage and an accumulation time of 40 s. Surface analysis of crystals typically showed an excess of the flux in which the crystal were synthesized, so EDS was performed on the interior of cleaved crystals to improve results.

2.2. Structure refinements

Samples for X-ray diffraction were selected from the SEM plate after elemental analysis. The large crystals were cleaved into smaller pieces, which were mounted on glass fibers. Single-crystal X-ray diffraction data were collected at room temperature using a Bruker AXS SMART CCD diffractometer equipped with a Mo radiation source; lattice constants are summarized in Table 1. Processing of the data was accomplished with use of the program SAINT; an absorption correction was applied to the data using the SADABS program [5]. Refinement of the structure was performed using the SHELXTL package [6]. The crystallographic data are summarized with four representative RMn$_2$Al$_x$Zn$_{20-x}$ and RMn$_2$In$_x$Zn$_{20-x}$ compounds listed in Table 2; the atomic positions are displayed in Table 3. Powder X-ray diffraction data were collected on several samples using a Rigaku Ultima III Powder X-ray diffractometer with a Cu radiation source and a CCD detector. Additional details regarding the crystallographic refinements can be obtained from the Fachinformationszentrum Karlsruhe, 76344 Eggenstein-Leopoldshafen, Germany (e-mail: crysdata@fiz.karlsruhe.de) on quoting the depository numbers 416909–416925.

2.3. Magnetic susceptibility

Magnetic measurements were carried out with a Quantum Design MPMS SQUID magnetometer at temperatures between 3 and 300 K. Crystals were first analyzed using EDS, then were sealed in kapton tape and placed into the magnetometer. Temperature-dependent susceptibility data were collected at 500 or 1000 G, and field dependence data were collected at 3 K. Magnetic measurements for many of the samples were complicated by complex nonlinear Curie–Weiss behavior indicative of a high amount of paramagnetic Mn-containing impurities and In inclusions.

Table 1
Lattice constants of the compounds RMn$_2$$Tr_xZn_{20-x}$

Compound	a (nm)	V (nm^3)	R_1 [$I>2\sigma(I)$][a]
YMn$_2$(In$_5$Zn$_{15}$)	14.7285(4)	3195.04(15)	.0274
CeMn$_2$(In$_{4.7}$Zn$_{15.3}$)	14.6786(2)	3162.67(7)	.0253
PrMn$_2$(In$_5$Zn$_{15}$)	14.7096(4)	3182.75(15)	.0278
NdMn$_2$(In$_{4.5}$Zn$_{15.5}$)	14.6522(6)	3145.64(2)	.0404
SmMn$_2$(In$_{5.9}$Zn$_{14.1}$)	14.8125(4)	3250.01(15)	.0234
GdMn$_2$(In$_{5.1}$Zn$_{14.9}$)	14.7629(6)	3217.47(2)	.0273
DyMn$_2$(In$_{4.7}$Zn$_{15.3}$)	14.6677(7)	3155.63(3)	.0280
ErMn$_2$(In$_{2.8}$Zn$_{17.2}$)	14.4419(4)	3012.13(14)	.0201
YbMn$_2$(In$_{5.5}$Zn$_{14.5}$)	14.7140(3)	3185.61(11)	.0249
YMn$_2$(Al$_{3.9}$Zn$_{16.8}$)	14.1533(3)	2835.13(10)	.0250
CeMn$_2$(Al$_{5.3}$Zn$_{14.7}$)	14.2489(4)	2892.71(14)	.0196
PrMn$_2$(Al$_{7.3}$Zn$_{12.7}$)	14.2670(2)	2904.01(7)	.0210
NdMn$_2$(Al$_{4.8}$Zn$_{15.2}$)	14.2499(2)	2893.58(7)	.0383
SmMn$_2$(Al$_{4.9}$Zn$_{15.1}$)	14.1740(14)	2847.59(5)	.0233
GdMn$_2$(Al$_5$Zn$_{15}$)	14.1761(8)	2848.86(3)	.0585
DyMn$_2$(Al$_{4.7}$Zn$_{15.3}$)	14.1438(4)	2829.43(14)	.0182
ErMn$_2$(Al$_{3.6}$Zn$_{16.4}$)	14.1287(4)	2820.37(14)	.0192
YbMn$_2$(Al$_{5.3}$Zn$_{14.7}$)	14.1152(3)	2812.30(10)	.0204

[a] $R_1 = \Sigma||F_o|-|F_c||/\Sigma|F_o|$.

Table 2
Crystal data for $CeMn_2(In_{4.7}Zn_{15.3})$, $SmMn_2(Al_{4.9}Zn_{15.1})$, $YbMn_2(In_{5.5}Zn_{14.5})$, and $YbMn_2(Al_{5.3}Zn_{14.7})$

	$CeMn_2(In_{4.7}Zn_{15.3})$	$SmMn_2(Al_{4.9}Zn_{15.1})$	$YbMn_2(In_{5.4}Zn_{14.5})$	$YbMn_2(Al_{5.3}Zn_{14.7})$
Formula weight (g/mol)	1656.30	1375.68	1689.22	1436.76
Space group	*Fd*-3*m*	*Fd*-3*m*	*Fd*-3*m*	*Fd*-3*m*
a (Å)	14.6786(2)	14.1740(14)	14.7140(3)	14.1152(3)
V (Å^3)	3162.67	2847.65	3185.61	2812.3
d_{calc} (g/cm^3)	6.957	6.418	7.044	6.787
Z	8	8	8	8
Temperature (K)	298	298	298	298
Radiation	Mo$K\alpha$	Mo$K\alpha$	Mo$K\alpha$	Mo$K\alpha$
$2\theta_{max}$	56.24	56.81	56.09	56.37
Index ranges	$-19 \leqslant h\,k\,l \leqslant 19$	$-18 \leqslant h\,k\,l \leqslant 18$	$-19 \leqslant h\,k\,l \leqslant 19$	$-18 \leqslant h\,k\,l \leqslant 18$
Reflections collected	10064	8731	10310	8991
Unique data/parameters	220/18	205/20	220/18	198/20
μ(mm^{-1})	33.865	30.759	36.635	35.221
R_1/wR_2* [$I > 2\sigma(I)$]	.0253/.0518	.0233/.0415	.0249/.0457	.0204/.0441
R_1/wR_2 (all data)	.0253/.0518	.0250/.0415	.0251/.0457	.0204/.0441
Residual peaks/hole	.764/−1.234	.953/−1.248	.874/−1.691	.925/−1.115

*$R_1 = \Sigma||F_o|-|F_c||/\Sigma|F_o|$; w$R_2 = [\Sigma[w(F_o^2-F_c^2)^2]/\Sigma[w(F_o^2)^2]]^{1/2}$.

Table 3
Atomic positions of $CeMn_2(In_{4.7}Zn_{15.3})$, $SmMn_2(Al_{4.9}Zn_{15.1})$, $YbMn_2(In_{5.5}Zn_{14.5})$, and $YbMn_2(Al_{5.3}Zn_{14.7})$

Atoms	Wyckoff site	x	y	z	Occup.	U_{eq}
$CeMn_2(In_{4.7}Zn_{15.3})$						
Ce	8*a*	1/8	1/8	1/8	1	.0046(4)
Mn	16*d*	1/2	1/2	1/2	1	.0047(6)
In1	16*c*	0	0	0	1	.0223(4)
Zn1	48*f*	.49291(10)	1/8	1/8	1	.0106(4)
In2	96*g*	.05696(4)	.05696(4)	.32973(6)	.225(9)	.0146(4)
Zn2	96*g*	.05696(4)	.05696(4)	.32973(6)	.775(9)	.0146(4)
$YbMn_2(In_{5.5}Zn_{14.5})$						
Yb	8*a*	1/8	1/8	1/8	1	.0079(3)
Mn	16*d*	1/2	1/2	1/2	1	.0064(6)
In1	16*c*	0	0	0	1	.0229(4)
Zn1	48*f*	.49327(9)	1/8	1/8	1	.0131(3)
In2	96*g*	.05756(4)	.05756(4)	.32854(6)	.295(9)	.0183(3)
Zn2	96*g*	.05756(4)	.05756(4)	.32854(6)	.705(9)	.0183(3)
$SmMn_2(Al_{4.9}Zn_{15.1})$						
Sm	8*a*	1/8	1/8	1/8	1	.0016(3)
Mn	16*d*	1/2	1/2	1/2	1	.0032(4)
Zn1	16*c*	0	0	0	.772(4)	.0145(7)
Al1	16*c*	0	0	0	.228(4)	.0145(7)
Zn2	96*g*	.05940(3)	.05940(3)	.32472(5)	.920(5)	.0077(3)
Al2	96*g*	.05940(3)	.05940(3)	.32472(5)	.080(5)	.0077(3)
Zn3	48*f*	.48695(9)	1/8	1/8	.410(4)	.0048(5)
Al3	48*f*	.48695(9)	1/8	1/8	.590(4)	.0048(5)
$YbMn_2(Al_{5.3}Zn_{14.7})$						
Yb	8*a*	1/8	1/8	1/8	1	.0011(3)
Mn	16*d*	1/2	1/2	1/2	1	.0014(5)
Zn1	16*c*	0	0	0	.77(1)	.0125(7)
Al1	16*c*	0	0	0	.23(1)	.0125(7)
Zn2	96*g*	.06009(4)	.06009(4)	.32301(5)	.940(8)	.0071(3)
Al2	96*g*	.06009(4)	.06009(4)	.32301(5)	.060(8)	.0071(3)
Zn3	48*f*	.48610(13)	1/8	1/8	.312(9)	.0044(6)
Al3	48*f*	.48610(13)	1/8	1/8	.688(9)	.0044(6)

3. Results and discussion

3.1. Synthesis

Synthesis in metal flux mixtures offers the opportunity to explore the comparative reactivity of two solvent metals and frequently allows lower temperature reactions due to the formation of eutectics. Removal of excess solvent by centrifugation is also facilitated by a low-melting eutectic. The behavior of pure zinc, aluminum, and indium fluxes has been well-studied. Zinc and aluminum are often incorporated into the intermetallic phases that crystallize from these solvents, forming zinc-rich phases (such as Co_2Zn_{15} and $EuZn_{13}$) [7] or aluminides (such as $CeAu_3Al_7$ and RNiAl$_4$Ge$_2$) [8]. Indium, on the other hand, appears to be a more inert solvent. While it has been used to synthesize indides such as $CeCoIn_5$ [9], it has also been used as a flux for the growth of indium-free silicides and germanides including $EuZn_2Si_2$, $La_2Zn_6Ge_3$, and β-DyNiGe$_2$ [10]. Si and Ge apparently form stronger interactions with the rare-earth and transition metal reactants than with In, so the flux is excluded from the final products. In the absence of a reaction directing main group element such as Si or Ge, it appears indium is more likely to be incorporated into products.

It is notable that the same structure and approximate stoichiometry forms from an indium-rich flux in the RMn$_2$In$_x$Zn$_{20-x}$ case and from a zinc-rich flux in the RMn$_2$Al$_x$Zn$_{20-x}$ case (x varies from 2 to 7 in both cases; see Table 1). After discovering these new compounds, reproducing and optimizing the In/Zn synthesis became quite a challenge. A large amount of RIn$_3$ was present as a secondary phase, evidenced in the X-ray powder diffraction data. With this information and the use of phase diagrams, it was decided to decrease the maximum temperature from 1000 to 900 °C; this helped remove the tendency for the reaction to form the more thermodynamically stable binary phase.

Once the yield of product was optimized, another problem became apparent. The rotation photographs of numerous samples (taken using the single-crystal X-ray diffractometer) showed streaks in addition to the sharper diffraction spots due to the crystal lattice. This was attributed to our samples forming inclusions of polycrystalline indium since there was a large excess of indium in the reaction. This is a common occurrence in certain flux systems and is a byproduct of excessive nucleation which occurs due to either too fast a cooling rate or too slow of a cooling rate [1]. The problem with inclusions was only apparent in the In/Zn synthesis; the Al/Zn synthesis products were free of such defects.

A variety of different transition metals were used in attempts to synthesize structural analogs in the In/Zn flux. Successful syntheses using an 8:2 In/Zn flux ratio occurred with the use of Mn and Fe, while Ti, V, Cr, Co, Ni, Cu, Rh, Ru, Ag, Au, Re, and Mo were all unsuccessful. Once all available transition metals were attempted, we began to develop analogs using other rare earths. We were successful in isolating RMn$_2$(In$_x$Zn$_{20-x}$) analogs with $R = Y$, Ce, Pr, Nd, Sm, Gd, Dy, Er, and Yb. Attempts to use La and Eu were unsuccessful, while Pm, Tb, Ho, Tm, and Lu were not available for use.

While synthesizing aluminum analogs using a Al/Zn flux ratio of 2:10, we were successful once again with Mn and Fe for the transition metals; for the rare-earth analogs we were successful with Y, Ce, Pr, Nd, Sm, Gd, Dy, Er, and Yb. Both RMn$_2$Al$_x$Zn$_{20-x}$ and RMn$_2$In$_x$Zn$_{20-x}$ compounds were unable to incorporate La and Eu, which may be due to size effects. Europium appears to favor the divalent state in many intermetallics; Eu^{2+} and La^{3+} have larger radii than the other rare-earth ions. Synthesis of similar compounds in Ga/Zn eutectic mixtures was not attempted due to the difficulty in distinguishing Ga and Zn in the X-ray structure, but it is expected that R(Mn/Fe)$_2$(Ga$_x$Zn$_{20-x}$) phases would form.

3.2. In/Zn compounds

The cubic RMn$_2$(Tr_xZn$_{20-x}$) structure (Fig. 1) can be viewed as a packing of coordination polyhedra with the rare-earth atoms coordinated by 16 Zinc/Tr atoms forming a Frank–Kasper polyhedron CN16 (Fig. 2(a)), while the transition metal rests inside a 12 coordinate icosahedron of Zn/Tr atoms (Fig. 2(b)). Upon comparison of the RMn$_2$(Tr)$_x$Zn$_{20-x}$ compounds to Jeitschko's RT_2Zn$_{20}$ compounds [4], we began to notice similarities and differences to our structures. There is some preferential siting seen in the indium phases, with indium occupying the 16c wyckoff site and Zn occupying the 48f site, but the 96g site is occupied by a mixture of In/Zn in all the analogs. The local environment of In1 (16c) consists of a double six-ring polyhedron, made from the mixed In2/Zn2 (96g) and

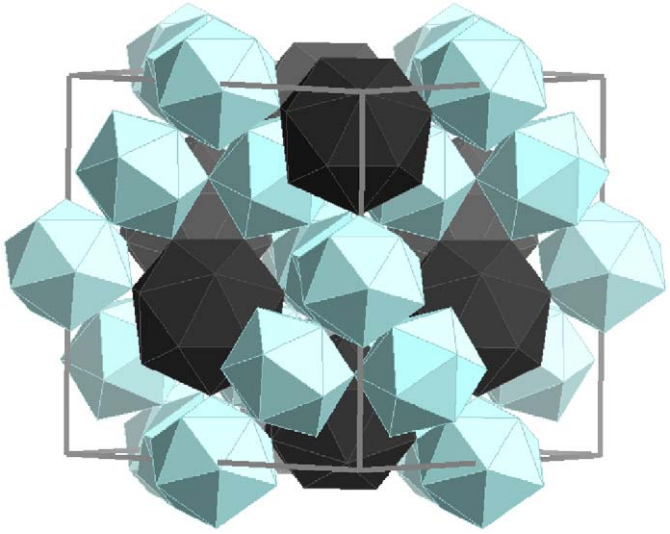

Fig. 1. The cubic RMn$_2$$Tr_xZn_{20-x}$ structure viewed down the [110] direction, showing the structure as connected polyhedra. The larger dark polyhedra (CN 16) contain the rare-earth element while the smaller light icosahedra (CN 12) are centered by the manganese atoms.

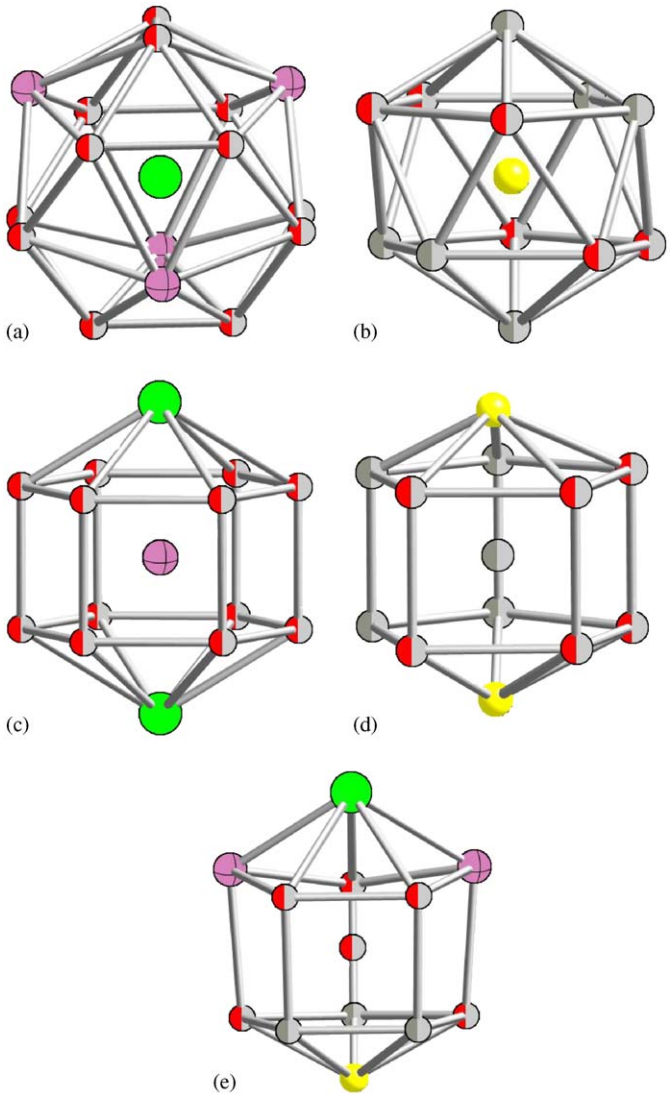

Fig. 2. Coordination polyhedra in the $RMn_2In_xZn_{20-x}$ compounds: (a) The rare-earth element R is represented by a large green sphere, (b) Mn is represented by a small yellow sphere, (c) In is represented by a large purple sphere with equatorial lines, (d) Zn1 is represented by small gray spheres, (e) the mixed In2/Zn2 site is represented by small half red half gray spheres.

Zn1 (48*f*) sites, capped axially by two rare-earth atoms (Fig. 2(c)). Indium favors this site likely due to the fact that it has a higher coordination number (CN 14) than either of the other two Zn sites (CN 12). Therefore, it can more readily accommodate the larger size of the indium atom. The Zn1 (48*f*) site rests inside a (CN 12) bicapped pentagonal prism with two transition metals in the axial position (Fig. 2(d)).

The local environment of the In2/Zn2 (96*g*) mixed site consists of a pentagonal prism of In and Zn comprised of the 96*g*, 48*f*, and 16*c* sites (Fig. 2(e)). The prism is capped axially by the transition metal and rare-earth with the rare-earth side being truncated. During the structural refinement, the occupancy of the 96*g* site was initially assigned to be filled with zinc. However, the occupancy was greater than 100%. Since these compounds were grown out of an indium flux, and indium has a higher scattering power than Zn, it was decided that perhaps this site was a mixed Zn/In occupancy. Upon examination of the thermal parameters for these sites, it was observed that the mixed site's thermal parameter was between the values for the pure In site and the pure Zn site, which further reinforced the idea that this was a mixed Zn/In site. The average indium occupancy on the 96*g* site for all analogs is $23.9\% \pm 7.4\%$.

After refinement of this mixed Zn/In site, it was observed that the unit cell volumes had a direct relationship to the amount of indium present in the sample (Fig. 3). This is reasonable given that indium's atomic radius (167 pm) is larger than the zinc radius of 134 pm and that indium is present in large amounts. Therefore, increasing or decreasing this amount would have a much larger effect on unit cell volume than the lanthanide contraction. For cases where the analogs have the same amount of indium incorporated in the structure, the cell volumes do appear to follow the lanthanide contraction.

The amount of indium present on the 96*g* site strongly impacts the local environments of the rare-earth (Fig. 2(a)) and transition metal (Fig. 2(b)). The rare-earth Frank–Kasper (CN 16) polyhedron is made up of elements from the mixed (In2/Zn2) 96*g* site and the In1 16*c* site. The 16*c* site of indium tetrahedrally coordinates to the rare-earth elements inside the (CN16) polyhedron. The *R*–In1 bond lengths show a linear dependence to the amount of indium present in the sample (Fig. 4). The *R*–(In2/Zn2) bond lengths show this dependence as well, but what is of notable interest is that the *R*–In1 bond lengths are shorter than the *R*–(In2/Zn2) bond lengths.

Upon examination of the icosahedral transition metal polyhedron (Fig. 2(b)), similar trends in bond lengths as stated earlier were observed. The transition metal polyhedron is surrounded by elements from the 96*g* mixed site (In2/Zn2) and the 48*f* zinc site (Zn1). The Mn–(In2/Zn2) bond length shows the linear dependence on bond length due to the amount of indium present in the sample; the

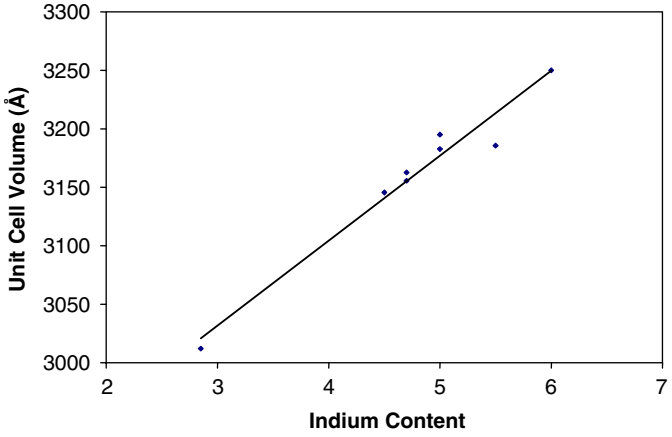

Fig. 3. Cell volumes of $RT_2In_xZn_{20-x}$ compounds versus amount of indium present in the sample.

Mn–Zn2 bond length (48*f* zinc site) shows this dependence as well even though it does not incorporate indium on the site. It was observed that as the indium content increased, the (In2/Zn2)–(In2/Zn2) bond lengths increased, as did the Zn1–(In2/Zn2) bond lengths; however, the Zn1–Zn1 bond lengths decreased (Fig. 5). This may be a compensation for the overall expansion of the polyhedra in the structure as the amount of indium rises.

3.3. Al/Zn compounds

Regarding the aluminum analogs (RMn$_2$Al$_x$Zn$_{20-x}$), the amount of aluminum on each of the three mixed sites can vary from 4% to 69% with no site having a preference for aluminum. This is reasonable considering the comparable size of atomic radii of aluminum (143 pm) and zinc (134 pm). Mn is again centering an icosahedron in this phase. The average Mn–Al2/Zn2 bond length for all the analogs is $275.9 \pm .5$ pm; clearly, there is very little variance in this bond length even though the amount of aluminum on this site can vary from 6% to 69%.

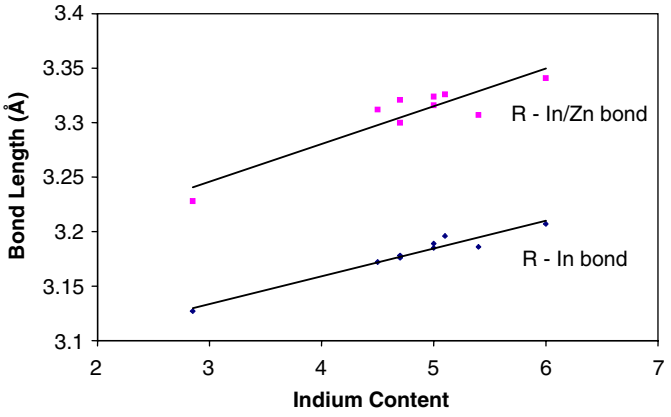

Fig. 4. Dependence of the *R*–In1 and *R*–(In2/Zn2) bond lengths in the rare-earth polyhedron on the indium content x of the compounds RMn$_2$In$_x$Zn$_{20-x}$.

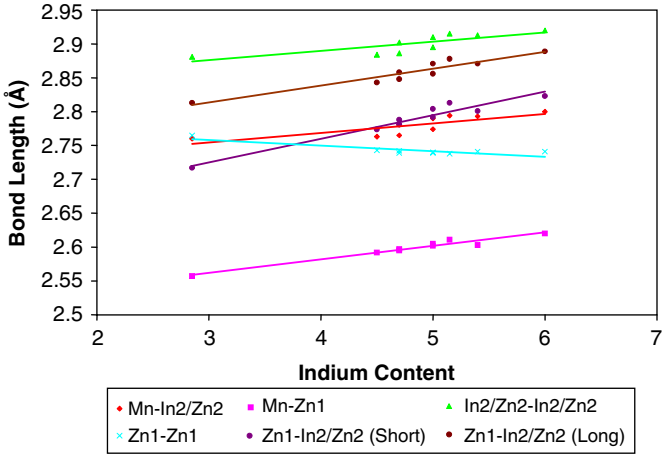

Fig. 5. Change in Mn icosahedron bond lengths due to varying amount of indium present in the RMn$_2$In$_x$Zn$_{20-x}$ compound.

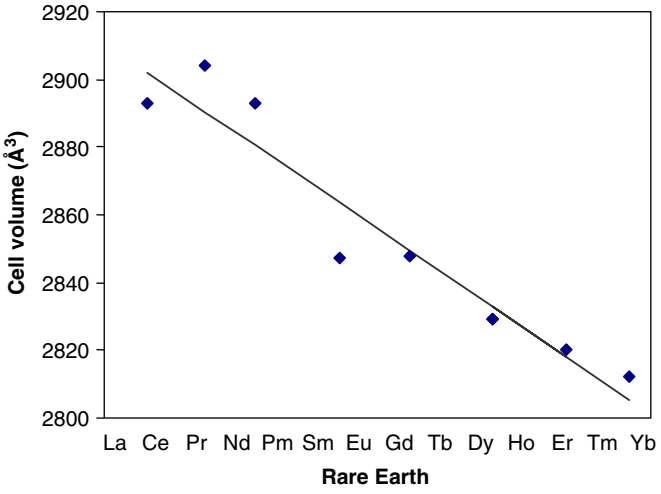

Fig. 6. Cell volumes of RMn$_2$Al$_x$Zn$_{20-x}$ versus rare-earth element size.

After refinement of these aluminum analogs, a trend in unit cell volumes became apparent. In this set of compounds, the cell volume no longer has a direct relationship to the amount of triel element in the mixed sites; it is apparent that the cell size of these analogs follows the lanthanide contraction (Fig. 6). This again can be attributed to aluminum's atomic radius being of comparable size to zinc's atomic radius; therefore, the larger perturbation caused by changing the rare-earth size governs volume effects.

3.4. Incorporation of manganese

Previous research has noted that RT_2Al$_{20}$ compounds [3] form with the early transition elements (T = Cr, Ti) whereas the RT_2Zn$_{20}$ compounds [4] incorporate the late transition elements (T = Fe, Co, Ni). This can be rationalized by atomic volume arguments. The polyhedra of these ternary structures are comprised of aluminum (with metallic radius of 143.2 pm) or zinc (with metallic radius of 139.4 pm). Therefore, assuming equally dense packing of the aluminum and zinc, the space available for the transition element is greater in the aluminides than in the zinc compounds [4]. Therefore, the larger early transition metals are accommodated in the aluminides, and the smaller late transition metals in the zinc phases.

This logic can be used to explain the incorporation of manganese in these RMn$_2Tr_x$Zn$_{20-x}$ compounds. The addition of a small amount of Al or In into the zinc framework creates a slightly expanded icosohedral coordination polyhedron which is large enough to contain Mn, but not large enough to incorporate the earlier transition metals. However, indium atoms are larger than aluminum atoms and one would expect that fewer In atoms need to be incorporated to allow for Mn inclusion if size were the dominant factor. But the amount of triel elements in these compounds averages around 5 for both the In- and Al-containing series. This indicates that another factor such as valence electron count (vec) may play a more important role.

Vec can account for Mn substitution, assuming Zn has two valence electrons and *Tr* elements have three. RT_2Zn_{20} compounds reported by Jeitschko have vec that vary between 59 and 63 as the identity of the transition metal and rare earth is varied [4]. For the $RMn_2Tr_xZn_{20-x}$ stoichiometry with x varying between 2 and 7 (as observed), calculated vec also range between 59 and 64, indicating a good fit to the stable vec range presented by Jeitschko. Unsubstituted RMn_2Zn_{20} (vec = 57) would fall outside this range. It appears that substitution of Zn by a triel element with a higher vec allows transition metals with lower vec to be incorporated into the structure.

3.5. Magnetic susceptibility

There is no evidence of magnetic ordering down to 3 K in any of the $RMn_2Tr_xZn_{20-x}$ compounds presented. This can be attributed to the large separation of the magnetic species (the rare-earth ions are over 6 Å apart); the lack of magnetic interactions is not unexpected. Compounds containing rare-earth metals with low magnetic moments (i.e., Ce^{3+}, Pr^{3+}) show slight deviations from Curie–Weiss behavior due to the presence of small amounts of paramagnetic Mn impurities; these were also apparent in the data for the analog containing non-magnetic Y^{3+}. The susceptibility of such impurities has a much less detrimental effect on the data for compounds of rare earths with larger magnetic moments, which display Curie–Weiss behavior. The magnetic moments derived from the data agree with the theoretical values for the rare-earth element, and the low Weiss constants are another indication of little to no interaction between magnetic ions. Magnetic susceptibility data for the $YbMn_2Al_{5.3}Zn_{14.7}$ analog are shown in Fig. 7(a); the fit indicates a trivalent state for ytterbium, with no sign of fluctuating or mixed valency (observed $\mu_{eff} = 5.01\,\mu_B$; theoretical μ_{eff} for $Yb^{3+} = 4.54\,\mu_B$). The data for $SmMn_2Al_{4.9}Zn_{15.1}$ are more complex, as shown in Fig. 7(b); it indicates that this compound strongly deviates from Curie–Weiss behavior. This is likely due to the complex van Vleck paramagnetism typically associated with Sm atoms in cubic symmetry [11].

Concurrence of the experimental magnetic moments with the theoretical values for the rare-earth ions indicates that the manganese atoms show diamagnetic behavior in these compounds. This is in agreement with studies of other multinary *R*/*T*/main group intermetallics containing low stoichiometric ratios of transition metals *T* [2d,8,10c]. Paramagnetic manganese is observed for intermetallic compounds that are comparatively rich in Mn; RMn_4Al_8 and RMn_6Al_6 have the same crystal structure, but only the latter material has magnetic Mn species.[12] On the other hand, Zintl phases (comprised of very electropositive metals—such as Na, Ca, Eu—in combination with main group metals or metalloids such as Tl, Ge, P, Bi) containing small amounts of Mn usually feature paramagnetic manganese ions, as seen in the compound $Ca_{14}MnP_{11}$.[13] However, these compounds are more ionic in nature and

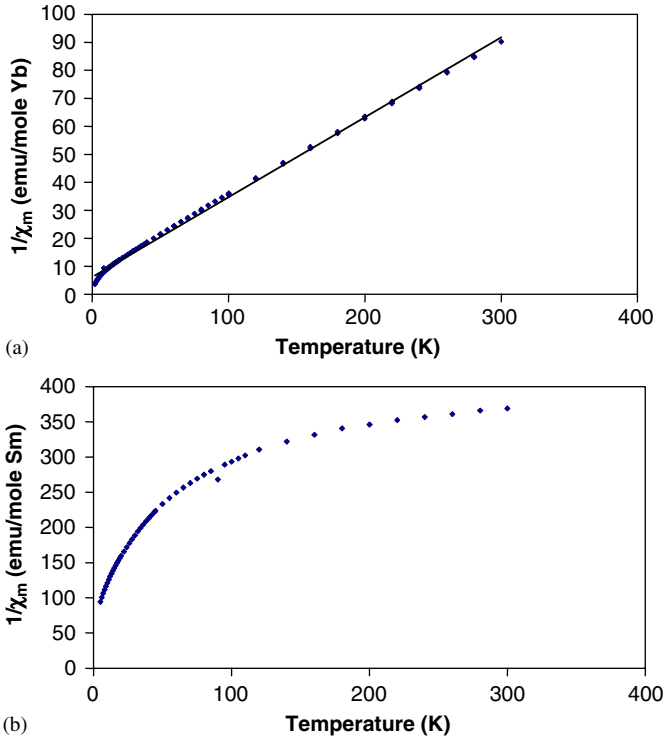

Fig. 7. Temperature dependence of the inverse molar susceptibility ($1/\chi_m$) for (a)$YbMn_2(Al_{5.3}Zn_{14.7})$ and (b) $SmMn_2(Al_{4.9}Zn_{15.1})$

lend themselves to being viewed as charge balanced materials with localized electrons producing a specific oxidation state/formal charge on each atom. Intermetallics such as the ones studied in this work can seldom be understood this way. While they may contain a very electropositive element whose oxidation state is obvious/measurable (such as Ca^{2+} or Nd^{3+}), the electrons donated by these elements are not localized on another specific atom or atoms in the structure; they are essentially delocalized in bands created by orbital overlap. The Mn *d*-band for the $RMn_2Tr_xZn_{20-x}$ structures is likely located below the Fermi level and will therefore be filled, rendering the Mn magnetically silent. Band structure calculations would be useful in studying this aspect of these compounds.

4. Conclusion

We have shown that mixed-metal fluxes are suitable media for the successful growth of $RMn_2Tr_xZn_{20-x}$, quaternary substituted variants of the ternary RT_2Tr_{20} structure. Substitution of zinc by a specific amount of triel (Al or In) produces the correct size and vec to allow the incorporation of Mn atoms into these phases. Although Fe analogs were also developed, they were not presented in this paper due to a variety of interesting structural features still under investigation, such as site switching behavior between the rare-earth and transition metal in some instances. This site switching also occurs between the Zn and In sites therefore changing the structure from high zinc

content to high indium content. These structures and a corresponding discussion will be followed up shortly once the new synthetic method has been optimized.

Acknowledgments

This research made use of the Scanning Electron Microscope facilities of MARTECH at Florida State University. Financial support from the ACS Petroleum Research Fund and the ORAU Ralph E. Powe Award are gratefully acknowledged. We thank Arris International for their generous gift of samarium.

References

[1] (a) Z. Fisk, J.P. Remeika, Handbook on the Physics and Chemistry of Rare Earths, vol. 12, G. Schneider, Eyring, 1989;
(b) P.C. Canfield, Z. Fisk, Philos. Mag. B 65 (1992) 1117;
(c) M.G. Kanatzidis, R. Pottgen, W. Jeitschko, Angew. Chem. Int. Ed. 44 (2005) 6996.

[2] (a) N. Gross, G. Block, W. Jeitschko, Chem. Mater. 14 (2002) 2725–2731;
(b) M.W. Wolff, S. Niemann, T. Ebel, W. Jeitschko, J. Magn. Magn. Mater. 223 (2001) 1–15;
(c) V.I. Zaremba, U. Rodewald, M. Lukachuk, V.P. Dubenskiy, B. Heying, K. Katoh, Y. Niide, A. Ochiai, R. Pottgen, Monats. Fur Chem. 137 (2006) 249–261;
(d) A. Szytula, J. Leciejewicz, Handbook of Crystal Structures and Magnetic Properties of Rare Earth Intermetallics, CRC Press, Boca Raton, FL, 1994.

[3] S. Niemann, W. Jeitschko, J. Solid State Chem. 114 (1995) 337.

[4] (a) T. Nasch, W. Jeitschko, U. Ch. Rodewald, Z. Naturforsch. 52b (1997) 1023;
(b) N. Gross, T. Nasch, W. Jeitschko, J. Solid State Chem. 161 (2001) 288–293.

[5] SAINT, version 6.02a,, Bruker AXS, Inc., Madison, WI, 2000.

[6] G.M. Sheldrick, SHELXTL NT/2000, version 6.1,, Bruker AXS, Inc., Madison, WI, 2000.

[7] M. Bostrom, S. Lidin, J. Solid State Chem. 166 (2002) 53–57.

[8] (a) S.E. Latturner, D. Bilc, J.R. Ireland, C.R. Kannewurf, S.D. Mahanti, M.G. Kanatzidis, J. Solid State Chem. 170 (2003) 48–57;
(b) B. Sieve, X. Chen, J. Cowen, P. Larson, S.D. Mahanti, M.G. Kanatzidis, Chem. Mater. 11 (1999) 2451–2455.

[9] R.T. Macaluso, J.L. Sarrao, P.G. Pagliuso, N.O. Moreno, R.G. Goodrich, D.A. Browne, F.R. Fronczek, J.Y. Chan, J. Solid State Chem. 166 (2002) 245–250.

[10] (a) A. Grytsiv, D. Kaczorowski, A. Leithe-Jasper, P. Rogl, C. Godart, M. Potel, H. Noel, J. Solid State Chem. 163 (2002) 37–43;
(b) A. Grytsiv, E. Bauer, S. Berger, G. Hilscher, H. Michor, C. Paul, P. Rogl, A. Daoud-Aladine, L. Keller, T. Roisnel, H. Noel, J. Phys. Condens. Matter 15 (2003) 3053–3067;
(c) J.R. Salvador, J.R. Gour, D. Bilc, S.D. Mahanti, M.G. Kanatzidis, Inorg. Chem. 43 (2004) 1403–1410.

[11] C. Kittel, Introduction to Solid State Physics, sixth ed, Wiley, New York, 1986, p. 405.

[12] N.P. Duong, J.C.P. Klaasse, E. Bruck, F.R. de Boer, K.H.J. Buschow, J. Alloys Compounds 315 (2001) 28–35.

[13] H. Kim, S. Kauzlarich, J. Solid State Chem. 178 (2005) 1935–1939.